



UNIVERSITY OF LEEDS

This is a repository copy of *Earliest land plants created modern levels of atmospheric oxygen*.

White Rose Research Online URL for this paper:
<http://eprints.whiterose.ac.uk/102812/>

Version: Accepted Version

Article:

Lenton, TM, Dahl, TW, Daines, SJ et al. (4 more authors) (2016) Earliest land plants created modern levels of atmospheric oxygen. *Proceedings of the National Academy of Sciences*, 113 (35). pp. 9704-9709. ISSN 0027-8424

<https://doi.org/10.1073/pnas.1604787113>

Reuse

Items deposited in White Rose Research Online are protected by copyright, with all rights reserved unless indicated otherwise. They may be downloaded and/or printed for private study, or other acts as permitted by national copyright laws. The publisher or other rights holders may allow further reproduction and re-use of the full text version. This is indicated by the licence information on the White Rose Research Online record for the item.

Takedown

If you consider content in White Rose Research Online to be in breach of UK law, please notify us by emailing eprints@whiterose.ac.uk including the URL of the record and the reason for the withdrawal request.



eprints@whiterose.ac.uk
<https://eprints.whiterose.ac.uk/>

Earliest land plants created modern levels of atmospheric oxygen

Timothy M. Lenton^{1*}, Tais W. Dahl², Stuart J. Daines¹, Benjamin J. W. Mills^{1,3}, Kazumi Ozaki⁴, Matthew R. Saltzman⁵, Philipp Porada⁶

¹Earth System Science, College of Life and Environmental Sciences, University of Exeter, Exeter EX4 4QE, UK. ²Natural History Museum of Denmark, Øster Voldgade 5-7, Copenhagen, Denmark. ³School of Earth and Environment, University of Leeds, Leeds LS2 9JT, UK. ⁴School of Earth and Atmospheric Sciences, Georgia Institute of Technology, 311 Ferst Drive, Atlanta, GA 30332-0340, USA. ⁵School of Earth Sciences, The Ohio State University, Columbus, Ohio 43214, USA. ⁶ Department of Environmental Science and Analytical Chemistry, Stockholm University, Svante Arrhenius väg 8, SE-114 18 Stockholm, Sweden.

Submitted to Proceedings of the National Academy of Sciences of the United States of America

The progressive oxygenation of the Earth's atmosphere was pivotal to the evolution of life, but the puzzle of when and how atmospheric oxygen (O₂) first approached modern levels (~21%) remains unresolved. Redox proxy data indicate the deep oceans were oxygenated during 435-392 Ma, and the appearance of fossil charcoal indicates O₂>15-17% by 420-400 Ma. However, existing models have failed to predict oxygenation at this time. Here we show that the earliest plants, which colonized the land surface from ~470 Ma onwards, were responsible for this mid-Paleozoic oxygenation event, through greatly increasing global organic carbon burial – the net long-term source of O₂. We use a trait-based ecophysiological model to predict that cryptogamic vegetation cover could have achieved ~30% of today's global terrestrial net primary productivity by ~445 Ma. Data from modern bryophytes suggests this plentiful early plant material had a much higher molar C:P ratio (~2000) than marine biomass (~100), such that a given weathering flux of phosphorus could support more organic carbon burial. Furthermore, recent experiments suggest that early plants selectively increased the flux of phosphorus (relative to alkalinity) weathered from rocks. Combining these effects in a model of long-term biogeochemical cycling, we reproduce a sustained +2‰ increase in the carbonate carbon isotope (δ¹³C) record by ~445 Ma, and predict a corresponding rise in O₂ to present levels by 420-400 Ma, consistent with geochemical data. This oxygen rise represents a permanent shift in regulatory regime to one where fire-mediated negative feedbacks on organic carbon burial stabilise high O₂ levels.

oxygen | plants | Paleozoic | phosphorus | weathering

Introduction

After the well-defined 'Great Oxidation Event' 2.45-2.32 Ga, the trajectory of atmospheric oxygen is deeply uncertain (1, 2). Many recent studies, reviewed in (3-5), have argued for a Neoproterozoic oxygenation event (>550 Ma) – of uncertain cause – and have linked it to the rise of animals, but this has been questioned given a lack of change in iron-speciation ocean redox proxy data (6). Some models predict pO₂ ~1 PAL (present atmospheric level) already in the early Paleozoic (7, 8), but this is at odds with data for widespread ocean anoxia (6, 9). The 'COPSE' model we adapt here (10) predicts early Paleozoic pO₂ ~0.2-0.5 PAL consistent with redox proxy data, but like the other models (7, 8) it does not predict a rise in oxygen until the advent of forests starting ~385 Ma, and continuing until ~300 Ma. This is too late to explain marked changes in geochemical data that occur before ~390 Ma (figure 1). The first appearance of fossil charcoal in the late Silurian (11) and its ongoing occurrence through the Devonian (12) (table S1), albeit rare and at low concentrations, indicates O₂>15-17% (by volume) of the atmosphere (13) (or O₂>~0.7 PAL assuming a constant N₂ reservoir) already by ~420-400 Ma. (Under ideal conditions of ultra-dry fuel and forced airflow, smoldering fires may be sustained at O₂>10%, but this is not believed to be possible under natural conditions (14)). The molybdenum

isotope record (9) indicates a fundamental shift in the redox state of the deep ocean from widespread anoxia to widespread oxygenation sometime during 435-392 Ma (between the early Silurian and the mid-Devonian). This ocean oxygenation is also supported by a Silurian increase in the C/S ratio of shales (15), and a shift in iron-speciation data sometime during 435-387 Ma (6).

The persistent oxygenation of the ocean and appearance of charcoal can be explained by a rise in atmospheric oxygen occurring by ~400 Ma. This could be due to a persistent increase in oxygen source – considered here – or a decrease in oxygen sink (16), leading to a reorganization of the Earth's surface redox balance at a higher steady-state level for atmospheric O₂. The major long-term source of oxygen to the atmosphere is the burial of organic carbon in sedimentary rocks (which represents the net flux of photosynthesis minus various pathways of respiration and oxidation). Increases in global organic carbon burial are recorded as positive shifts in the isotopic composition of carbonate rocks (δ¹³C). Consistent with a rise in oxygen, the carbon isotope record (17) (figure 1) indicates a fundamental shift in baseline from ≤0‰ prior to the Late Ordovician to ~2‰ from ~445 Ma onwards. Whilst there are many subsequent δ¹³C fluctuations, including drops back to 0‰, e.g. at ~400 Ma, the long-term mean δ¹³C remains ~2‰ throughout the rest of the Paleozoic, the Mesozoic, and the early Cenozoic (17), indicating a sustained increase in

Significance

The rise of atmospheric oxygen over Earth history has received much recent interdisciplinary attention. However, the puzzle of when and how atmospheric oxygen reached modern levels remains unresolved. Many recent studies have argued for a major oxygenation event - of uncertain cause - in the Neoproterozoic Era >541 million years ago (Ma), enabling the rise of animals. Previous modelling work has predicted a late Paleozoic oxygen rise (<380 Ma) due to the rise of forests. Here we show that neither scenario is correct. Instead the earliest plants, which colonized the land from 470 Ma onwards, first increased atmospheric oxygen to present levels by 400 Ma. This instigated fire-mediated feedbacks that have stabilised high oxygen levels ever since, shaping subsequent evolution.

Reserved for Publication Footnotes

137
138
139
140
141
142
143
144
145
146
147
148
149
150
151
152
153
154
155
156
157
158
159
160
161
162
163
164
165
166
167
168
169
170
171
172
173
174
175
176
177
178
179
180
181
182
183
184
185
186
187
188
189
190
191
192
193
194
195
196
197
198
199
200
201
202
203
204

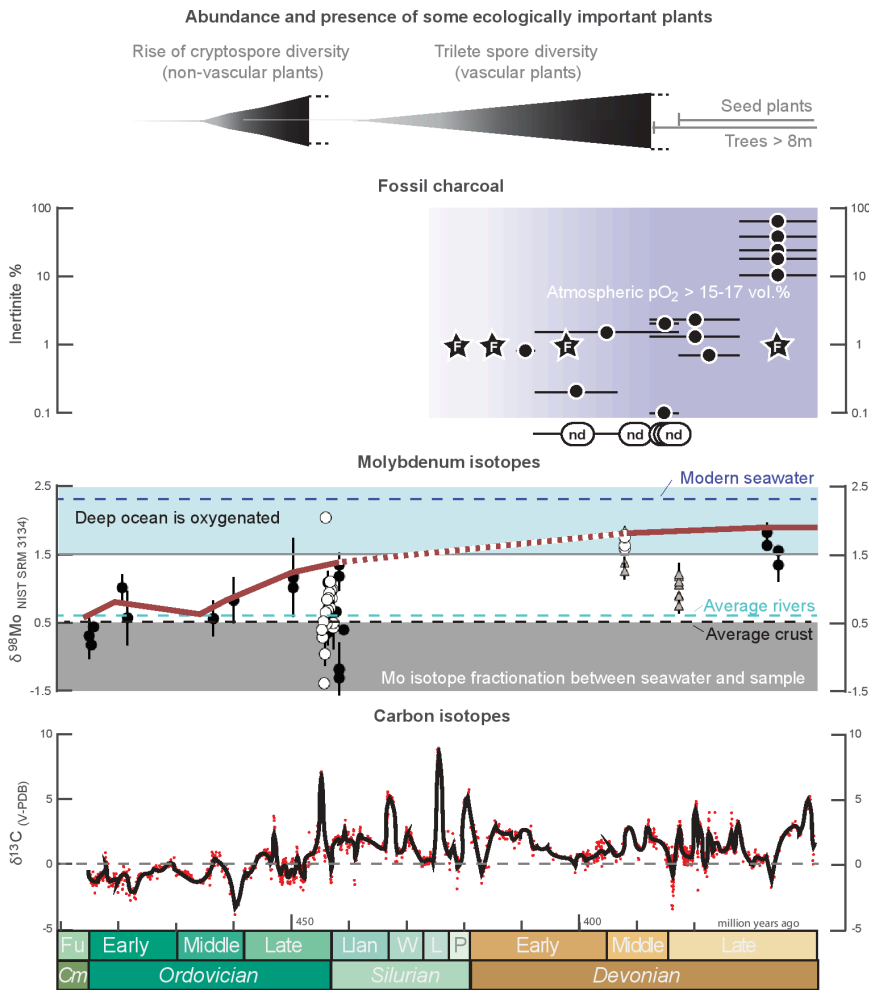


Fig. 1. Global changes during the Ordovician, Silurian, and Devonian Periods. The rise of non-vascular plants (indicated by cryptospore diversity (32)) then vascular plants (indicated by trilete spore diversity (18)) overlaps with the first appearances of fossil charcoal (table S1); F = fossils, black dots = inertinite in coal, nd = none detected. Molybdenum isotope data (9) indicate oxygenation of the deep ocean, following an uncertain trajectory ~440-390 Ma; black circles = euxinic shales as defined by Fe-speciation, white circles = euxinic shales as defined by Mo-enrichment, grey triangles = ferruginous shales as defined by Fe-speciation, blue area = isotope offset from oceanic input that requires a substantial Mn-oxide sink in the deep oceans. The carbonate carbon isotope record (17) (red dots, black line is a smoothed spline fit) indicates elevated organic carbon burial ($\delta^{13}\text{C} \sim 2\text{‰}$) ~445-410 Ma. Cm=Cambrian, Fu=Furongian, Llan=Llandovery, W=Wenlock, L=Ludlow, P=Pridoli.

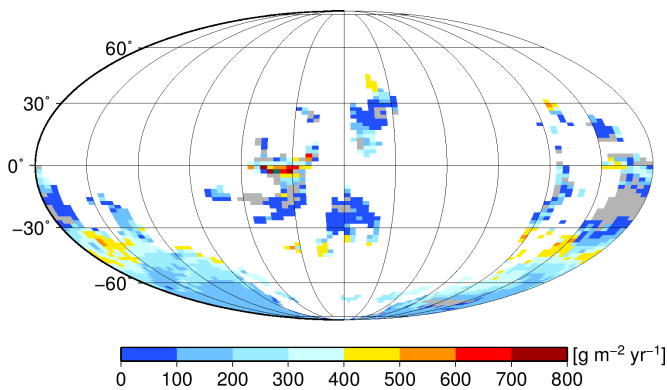


Fig. 2. Predicted Late Ordovician (445 Ma) net primary production (NPP). Result from ecophysiological model of cryptogamic vegetation cover driven by simulated Late Ordovician (445 Ma) climate, atmospheric $\text{CO}_2 = 8 \text{ PAL}$, and atmospheric $\text{O}_2 = 0.6 \text{ PAL}$ (14 vol.%), with no ice sheet mask. Simulated global NPP = 18.7 GtC yr^{-1} .

global organic carbon burial. Such a permanent shift requires a unidirectional driver that kicked-in during the mid-Paleozoic. The evolution of land plants is the obvious candidate, with the first non-vascular plants (ancestors of extant mosses, liverworts and hornworts) colonizing the land in the Mid-Late Ordovician (~470-445 Ma), followed by the first vascular plants in the Sil-

urian (~445-420 Ma) and early Devonian (~420-390 Ma) (figure 1) (18, 19).

Here we hypothesize that the evolution of these earliest land plants permanently increased organic carbon burial causing atmospheric oxygen to approach modern levels by ~400 Ma, and creating a new dynamically stable steady state for the oxygen cycle (where the major long-term O_2 sink from oxidative weathering of ancient organic carbon increased to counterbalance the increased O_2 source). In simple terms, on long timescales, the global organic carbon burial flux is determined by the supply flux of the ultimate limiting nutrient phosphorus from weathering and the (molar) ratio of carbon-to-phosphorus in material that is buried:

$$\text{P weathering flux} \times \text{C}_{\text{organic}}/\text{P}_{\text{total}} \text{ burial ratio} = \text{C}_{\text{organic}} \text{ burial flux}$$

Land plants typically have a much higher molar C/P ratio (~1000) than marine organic matter (~100) due to carbon-rich but phosphorus-poor structural compounds such as sporopollenin, lignin and, in their fungal mycorrhizal symbionts, chitin. Therefore they can support an increased organic carbon burial flux for the same P weathering flux. The P weathering flux is partly tied to bulk silicate weathering, e.g. due to the dissolution of apatite inclusions in silicate rocks, and the silicate weathering flux of alkalinity is in turn set by negative feedback in the long-term carbon cycle, so is ultimately controlled by the degassing input of CO_2 on timescales $\geq 1 \text{ Myr}$ (7, 10). However, plants and their associated mycorrhizal fungi can increase phosphorus weathering

205
206
207
208
209
210
211
212
213
214
215
216
217
218
219
220
221
222
223
224
225
226
227
228
229
230
231
232
233
234
235
236
237
238
239
240
241
242
243
244
245
246
247
248
249
250
251
252
253
254
255
256
257
258
259
260
261
262
263
264
265
266
267
268
269
270
271
272

273
274
275
276
277
278
279
280
281
282
283
284
285
286
287
288
289
290
291
292
293
294
295
296
297
298
299
300
301
302
303
304
305
306
307
308
309
310
311
312
313
314
315
316
317
318
319
320
321
322
323
324
325
326
327
328
329
330
331
332
333
334
335
336
337
338
339
340

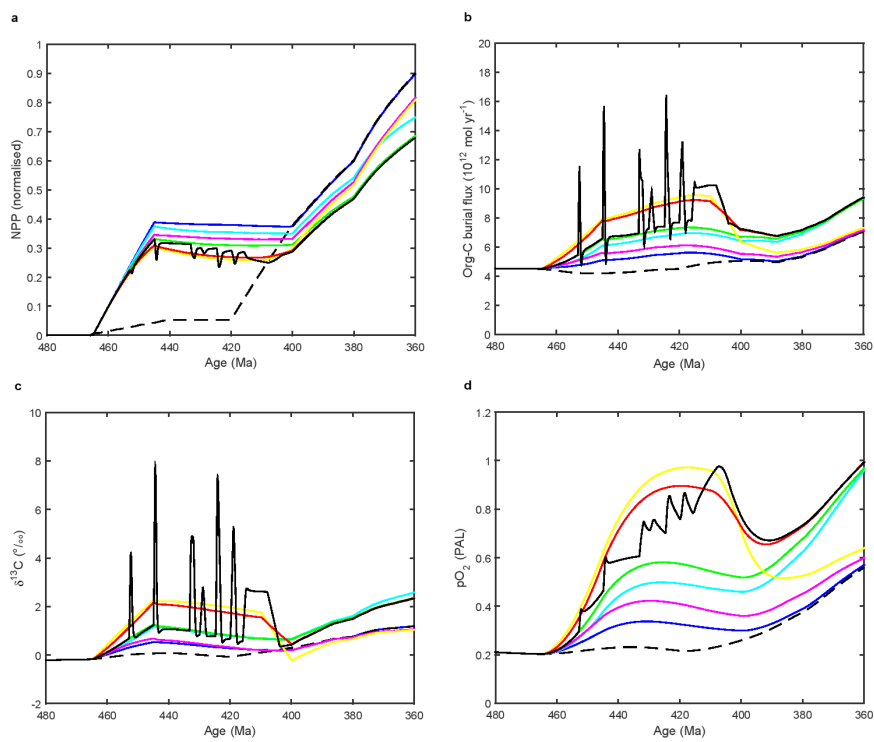


Fig. 3. Predictions of mid-Paleozoic global carbon cycle change due to early plants from the updated COPSE model: **a.** Net primary production (NPP); **b.** Organic carbon burial (both terrestrial and marine derived material); **c.** Carbonate carbon isotope record ($\delta^{13}\text{C}$); **d.** Atmospheric O_2 . Note that fossil charcoal 420-400 Ma indicates $\text{O}_2 > 0.66\text{-}0.77$ PAL. (Further results of the same model runs are in figures S3 and S5.) Black dashed = original baseline model run. Blue = early plant colonization ($\text{C}/\text{P}=1000$). Cyan = early plant colonization + $\text{C}/\text{P}=2000$. Magenta = early plant colonization + biotic effects on silicate weathering ($\text{C}/\text{P}=1000$). Green = early plant colonization + $\text{C}/\text{P}=2000$ + biotic effects on silicate weathering. Yellow = early plant colonization + biotic effects on silicate weathering + 50% increase in P weathering. Red = early plant colonization + $\text{C}/\text{P}=2000$ + biotic effects on silicate weathering + 25% increase in P weathering. Black = early plant colonization + $\text{C}/\text{P}=2000$ + biotic effects on silicate weathering + spikes of P weathering.

(20-22), and this could be sustained on longer timescales if they preferentially weather phosphorus relative to alkalinity.

In existing models, the evolution of trees starting ~ 385 Ma is assumed to have led to the burial of high C/P organic material in coal swamps (7, 8, 10), potentially augmented by increased phosphorus weathering rates (10). The Carboniferous-Permian peak in coal production has often been attributed to the evolution of lignin synthesis and a lag before the evolution of fungal degradation of lignin (23), but recent work has questioned this (24). Earlier plants possessed lignified 'woody' tissue (25), with precursor structures existing in marine algae before the transition to land (26), and lignin-degrading fungi potentially present before the Carboniferous (24). Carboniferous coals are not dominated by lignin, instead their accumulation was controlled by a combination of climate and tectonics supporting the creation and sedimentary preservation of peat bogs (24, 27). Given that earlier plants developed peatlands (28), and had rock weathering capabilities (20, 21), they could also have affected the global carbon cycle (18, 20).

Results and discussion

To test our hypothesis we revised the COPSE biogeochemical model (10) to better capture the early rise of plants and examine under what conditions it could explain the geochemical data (persistent rise to $\delta^{13}\text{C} \sim 2\text{‰}$ and the appearance of charcoal). The original baseline model (10) predicts early Paleozoic $\text{O}_2 \sim 0.23$ PAL at a reference time of 445 Ma, supported by an organic carbon burial flux of $\sim 4 \times 10^{12}$ mol yr^{-1} (about half the present day value) with $\delta^{13}\text{C} = 0.03\text{‰}$. In this stable state, oxidative weathering of ancient organic carbon is correspondingly reduced and its sensitivity to changes in O_2 provides a key negative feedback stabilizing O_2 . Key assumptions going into altering the forcing of the model are the global extent and associated productivity of early plants, the C/P ratio of plant material that was buried, and their effect (if any) on phosphorus weathering. To help parameterize these factors we drew on a mixture of experiments, existing data, and more detailed spatial modelling.

We used a trait-based spatial model of cryptogamic vegetation (i.e. bryophyte and lichen) cover (29, 30) driven by Late Ordovician climate simulations (31) at different atmospheric CO_2 levels to predict the potential global net primary productivity (NPP) of the early plant biosphere (32). At atmospheric $\text{CO}_2 = 8$ PAL, consistent with Late Ordovician glaciations (20), predicted global NPP is ~ 19 GtC yr^{-1} (figure 2), $\sim 30\%$ of today. Predicted NPP is sensitive to variations in CO_2 and climate (figure S1), ice sheet cover (figure S2), and O_2 (table S2), and is consistently higher than the 4.3 GtC yr^{-1} (7% of today) estimated elsewhere (33). In the original COPSE model (10), predicted NPP only reaches $\sim 5\%$ of today's value in the Late Ordovician and Silurian, but when we assume a stronger late Ordovician phase of land colonization by non-vascular plants (following (20), see SI), then COPSE predicts global NPP 30-40% of today (figure 3a), consistent with the detailed spatial model. In COPSE, this advent of early land plants alone, with no assumed effect on weathering fluxes, and assumed $\text{C}/\text{P}=1000$, increases total organic carbon burial by $\sim 25\%$, $\delta^{13}\text{C}$ by 0.5‰, and atmospheric O_2 by 0.11 PAL (figure 3, blue).

We undertook a literature review of molar C/P ratios in extant bryophytes (table S3) to test whether $\text{C}/\text{P}=1000$ is a reasonable assumption for early plants. This gives a range of $\text{C}/\text{P}=800\text{-}4300$ with a mean of $\text{C}/\text{P} \sim 1900$. Furthermore, early Devonian coaly shales indicate extensive peatlands 410-400 Ma and have C/N of 44-119 (28), comparable to that in modern peatlands where N/P and C/P ratios tend to increase with depth to $\text{C}/\text{P} > 3000$ (34). Taken together these data suggest that assuming $\text{C}/\text{P}=1000$ for early plants is conservative. If instead we assume that buried early plant matter had $\text{C}/\text{P}=2000$, then given their productivity, even with no effect on weathering fluxes, this increases global organic carbon burial by $\sim 50\%$, $\delta^{13}\text{C}$ by 1.1‰ and atmospheric O_2 by 0.27 PAL (figure 3, cyan).

Early plants could also have had a significant effect on weathering fluxes (20), as they and their fungal mycorrhizal symbionts evolved means of accessing rock-bound nutrients, notably phosphorus. Experimental work (20) has shown that a modern

341
342
343
344
345
346
347
348
349
350
351
352
353
354
355
356
357
358
359
360
361
362
363
364
365
366
367
368
369
370
371
372
373
374
375
376
377
378
379
380
381
382
383
384
385
386
387
388
389
390
391
392
393
394
395
396
397
398
399
400
401
402
403
404
405
406
407
408

409 non-vascular plant, the moss *Physcomitrella patens* amplifies the
410 weathering of Ca ions 1.4-3.6 fold and Mg ions 1.5-5.4 fold from
411 silicate rocks (granite-andesite), and amplifies the weathering
412 of phosphorus from granite ~24(15-43) fold (see Materials and
413 Methods). Subsequent experiments (21) with the modern liver-
414 wort *Marchantia paleacea* found a 2.5-7 fold amplification of Ca
415 weathering and a 9-13 fold amplification of P weathering from
416 basalt. Both studies thus indicate preferential weathering of P
417 relative to Ca and Mg (and corresponding alkalinity). The pres-
418 ence of these rock weathering capabilities in two early-diverging
419 lineages (mosses and liverworts) suggests it is an ancestral trait.
420 It has been argued (21, 33) that such large measured local effects
421 would not have scaled up to significant global effects, because of
422 low global NPP (33) and a limited depth of influence in the soil
423 (21). However, we estimate much higher global NPP (figure 2)
424 and weathering potential (32). We also note that extensive shallow
425 water phosphate deposits in the Late Ordovician (35) indicate a
426 marked increase in phosphorus input to the ocean (20).

427 If we include in COPSE an effect of early plants on silicate
428 weathering following (20), assuming C/P=1000, this increases
429 organic carbon burial by ~35%, $\delta^{13}\text{C}$ by 0.7‰, and O_2 by 0.18
430 PAL (figure 3, magenta). The effect on O_2 is constrained because
431 atmospheric CO_2 and temperature are reduced (20) such that
432 the silicate weathering flux (and associated phosphorus flux)
433 continues to match the degassing flux of CO_2 (figure S3). How-
434 ever, increases in carbonate weathering (enhanced by plants) and
435 oxidative weathering (due to the rise in O_2) increase the overall
436 phosphorus weathering flux, roughly doubling the O_2 rise due to
437 terrestrial production of high C/P material alone. Assuming that
438 buried early plant matter had a higher C/P=2000 causes larger
439 increases in total organic carbon burial ~60%, $\delta^{13}\text{C}$ +1.2‰, and
440 atmospheric O_2 +0.35 PAL (figure 3, green).

441 However, to reproduce the observed $\delta^{13}\text{C}$ +2‰ excursion
442 requires the inclusion of some selective weathering of phosphorus
443 by early plants. Assuming that early plants caused a sustained
444 50% increase in phosphorus weathering relative to bulk rock
445 dissolution, with C/P=1000, increases total organic carbon burial
446 by ~95%, $\delta^{13}\text{C}$ by 2.2‰ and O_2 by 0.74 PAL (to 0.97 PAL at
447 417 Ma) (figure 3, yellow). Assuming a sustained 25% increase
448 in phosphorus weathering relative to bulk rock and C/P=2000,
449 increases organic carbon burial by ~90%, $\delta^{13}\text{C}$ by 2.1‰ and O_2
450 by 0.67 PAL (figure 3, red). Alternatively, a series of P weathering
451 spikes designed to reproduce the observed sequence of positive
452 $\delta^{13}\text{C}$ excursions (figure 1), combined with C/P=2000, produces
453 a series of spikes in organic carbon burial and a peak increase
454 of O_2 of 0.72 PAL at 407 Ma (figure 3, black). We hypothesize
455 that these assumed weathering spikes could reflect phases of plant
456 colonization (20, 36) followed by the establishment of phosphorus
457 recycling ecosystems (20). However, direct evidence linking a
458 phase of land colonization to enhanced weathering and a positive
459 $\delta^{13}\text{C}$ excursion has only thus far been established for the Silurian-
460 Devonian boundary excursion (36). Therefore alternative hy-
461 potheses for short-lived positive $\delta^{13}\text{C}$ excursions should also be
462 considered.

463 Regarding the simulated long-term ~2‰ rise in $\delta^{13}\text{C}$ this
464 is smaller than would be expected from standard application
465 of the simplified formula: $\delta^{13}\text{C}(\text{ocean}) = \delta^{13}\text{C}(\text{river}) + f_{\text{org}} \cdot \epsilon$,
466 where f_{org} is the fraction of carbon buried as organic matter,
467 ϵ is the fractionation between carbonates and organic matter,
468 and both ϵ and $\delta^{13}\text{C}(\text{river})$ are usually assumed to be constant.
469 In our COPSE simulations there is a fully interactive isotope
470 mass balance and these terms are not constant. The approximate
471 doubling of organic carbon burial (with roughly constant car-
472 bonate burial) represents an increase from $f_{\text{org}} = 0.18$ to $f_{\text{org}} =$
473 0.31. However, the increase in burial of isotopically-light organic
474 carbon is counteracted by an increase in the oxidative weathering

475 of isotopically-light organic carbon, which lowers the $\delta^{13}\text{C}$ of
476 riverine input to the ocean from ca. -5‰ to ca. -7.5‰. This in turn
477 is partially counteracted by an increase in fractionation between
478 carbonates and organic matter from $\epsilon \sim 27\text{‰}$ to $\epsilon \sim 30\text{‰}$, due to
479 increasing O_2 (somewhat counteracted by declining CO_2).

480 Sensitivity analyses (see SI) indicate that our results are
481 robust. Varying the uplift and degassing forcing of the model
482 within plausible bounds only causes ± 0.08 PAL variation in O_2
483 about the initial state (figure S4), although it does cause the effect
484 of the same early plant forcing scenario to range over +0.4-1.0
485 PAL O_2 (table S4). Including an additional negative feedback on
486 O_2 , from increased marine organic C/P burial ratios under anoxic
487 waters (37), increases its initial early Paleozoic level to 0.54 PAL
488 and reduces the effect of the same biological forcing scenarios
489 on O_2 by ~10-30%, giving a maximum increase of +0.63 PAL
490 (table S5). However, because the initial O_2 is now higher, the
491 final O_2 is also higher in all cases, and even scenarios without
492 selective weathering of phosphorus could explain the appearance
493 of charcoal ($\text{O}_2 > \sim 0.7$ PAL).

494 Our model makes additional predictions that can be tested
495 against geochemical data, notably it predicts a decline in pyrite
496 sulfur burial and associated drop in $\delta^{34}\text{S}$ and increase in seawater
497 $[\text{SO}_4]$ and C/S burial ratio with the rise of the earliest plants
498 (figure S5). This is broadly consistent with the sulfur isotope
499 ($\delta^{34}\text{S}$) record (38-40), which shows a marked decline through the
500 Silurian-early Devonian from ~30‰ to ~18‰, although available
501 data also suggest an earlier late Ordovician-early Silurian rise
502 from ~25‰ to ~30‰, which the present model does not capture.
503 The model is consistent with proxy reconstructions of seawater
504 $[\text{SO}_4]$, which suggest an Ordovician-Silurian rise from ~6 mM to
505 ~10 mM (41), and with a Silurian increase in the molar C/S ratio
506 of shales from ~5 to ~16 (15).

507 Other processes not yet included in the model warrant future
508 consideration, for example the effect of increasing atmospheric
509 mass on climate (42), and the effect of weathering forcing sce-
510 narios on $\delta^7\text{Li}$ and $^{87}\text{Sr}/^{86}\text{Sr}$, which enable additional tests against
511 data.

512 Conclusion

513 Our model can only reproduce Paleozoic geochemical data if
514 the rise of the earliest land plants caused a major oxygenation
515 event of the Earth's atmosphere and oceans by ~400 Ma. We
516 attribute this mid-Paleozoic oxygenation event to a persistent
517 global increase in organic carbon burial supported by the high C/P
518 ratio of early land plant material, augmented by a plant-driven
519 increase in P weathering flux relative to the weathering flux of al-
520 kalinity. The $\delta^{13}\text{C}$ record suggests this increase in organic carbon
521 burial was essentially permanent, producing a new dynamically
522 stable state for atmospheric O_2 . In this new steady state, oxidative
523 weathering was increased (becoming less sensitive to variations
524 in O_2) and new fire-mediated negative feedbacks on O_2 were
525 instigated that have played a key role in stabilising atmospheric
526 O_2 concentration up to the present day (22, 43). For the earliest
527 land plants to be responsible for such a major mid-Paleozoic
528 oxygenation event requires that they were much more productive
529 and globally extensive than has been previously assumed (7, 10,
530 33). This hypothesis makes testable predictions with regard to
531 effects on other biogeochemical cycles, notably sulfur. If it stands
532 up to further scrutiny, then we can infer that the earliest land
533 plants created a stable oxygen-rich atmosphere that was necessary
534 for the subsequent evolution of large, mobile, intelligent animals
535 with a high respiratory oxygen demand – including ourselves.

536 Materials and Methods:

537 **Data compilation:** The early charcoal record (table S1) was compiled from
538 the literature (11, 12, 28, 44-72), utilizing existing compilations (12, 44-
539 47) and checking them where possible against the original sources. This
540 involved some reconciling of disparate results between existing compilations
541 and revision of some erroneous quoted values. Where recalculations were

warranted, inertinite percentages were calculated on a mineral-matter-free (mmf) basis, following (45, 47).

The molybdenum isotope record from marine shales was updated from (9) with data from (73, 74). Uncertainties shown in figure 1 represent 2 standard deviation of the mean (analytical precision) plus the propagated uncertainty from matching in-house reference materials to the universal standard NIST SRM 3136 where seawater display $\delta^{98/95}\text{Mo} = 2.3\text{‰}$ (see (75, 76)). The redox state of the host shales was determined using either Fe-speciation or Mo-enrichment proxies. Euxinic shales are defined (77) by the Fe-speciation proxy when $\text{FeHR}/\text{FeT} > 0.38$ and $\text{FeP}/\text{FeHR} > 0.7$ (black circles in figure 1). Euxinic shales are defined (78, 79) by the Mo enrichment proxy when $\text{Mo} > 25$ ppm (white circles in figure 1). Ferruginous shales (77) are defined by the Fe speciation proxy when $\text{FeHR}/\text{FeT} > 0.38$ and $\text{FeP}/\text{FeHR} < 0.7$.

The carbon isotope record (17) was fitted with a smoothed spline function in Matlab; spline = csaps(age, $\delta^{13}\text{C}$, rho), where $\rho = 0.99$ (close to data, but the curve in figure 1 does not go through each data point).

The C/P ratio of extant bryophytes (table S3) was compiled from data in the literature (34, 80-88). Where only values of mg P/g biomass were available, a value of mg C/g biomass = 430 was assumed based on the mean value across 6 bryophyte species from (89). Results for molar C/P ratios are given to 2 significant figures, given the uncertainty in the input data, except where authors themselves provide more precise values.

Ecophysiological model of cryptogamic vegetation: We used a trait-based spatial model of cryptogamic vegetation (i.e. bryophyte and lichen) cover to estimate the potential global net primary productivity (NPP) of the early non-vascular plant biosphere (29, 30). The Late Ordovician (445 Ma, Hirnantian Stage) setup of the model is fully described elsewhere (32). The model is driven by existing Late Ordovician climate simulations (31), conducted at a range of different atmospheric CO_2 and O_2 concentrations. Initially, we assume atmospheric $\text{O}_2 = 0.6$ PAL (~ 14 vol.%) at 445 Ma, which is consistent with those COPSE model simulations (figure 3d) that go on to produce O_2 levels consistent with the fossil charcoal record. We also initially assume atmospheric $\text{CO}_2 = 8$ PAL, which is a widely quoted value consistent with the occurrence of Hirnantian glaciations at 445 Ma (20), and is consistent with those COPSE model simulations that assume an effect of early plants on silicate weathering following (20). We explored the sensitivity of predicted global NPP to variations in atmospheric CO_2 and corresponding climate state (figure S1), to constraining vegetation cover with extensive Late Ordovician ice sheet cover (figure S2), and to varying O_2 in combination with CO_2 (table S2). The relatively high global NPP results obtained are consistent with present day cryptogamic covers providing $\sim 7\%$ of global NPP, despite making up only 1% of terrestrial vegetation by mass (90), and being restricted to relatively resource-poor habitats, whilst also operating in an atmosphere with a low CO_2/O_2 ratio.

1. Canfield DE (2014) Proterozoic Atmospheric Oxygen. *Treatise on Geochemistry. 2nd Edition*, eds Holland HD & Turekian KK (Elsevier Science, Oxford), Vol 6, pp 197-216.
2. Lyons TW, Reinhard CT, & Planavsky NJ (2014) The rise of oxygen in Earth's early ocean and atmosphere. *Nature* 506(7488):307-315.
3. Lenton TM, Boyle RA, Poulton SW, Shields GA, & Butterfield NJ (2014) Co-evolution of eukaryotes and ocean oxygenation in the Neoproterozoic era. *Nature Geoscience* 7(4):257-265.
4. Shields-Zhou GA & Och LM (2011) The case for a Neoproterozoic Oxygenation Event: Geochemical evidence and biological consequences. *GSA Today* 21(3):4-11.
5. Och LM & Shields-Zhou GA (2012) The Neoproterozoic oxygenation event: Environmental perturbations and biogeochemical cycling. *Earth-Science Reviews* 110(1-4):26-57.
6. Sperling EA, et al. (2015) Statistical analysis of iron geochemical data suggests limited late Proterozoic oxygenation. *Nature* 523(7561):451-454.
7. Berner RA (2006) GEOCARBSULF: A combined model for Phanerozoic atmospheric O_2 and CO_2 . *Geochimica et Cosmochimica Acta* 70(23):5653-5664.
8. Berner RA & Canfield DE (1989) A new model for atmospheric oxygen over Phanerozoic time. *American Journal of Science* 289:333-361.
9. Dahl TW, et al. (2010) Devonian rise in atmospheric oxygen correlated to the radiations of terrestrial plants and large predatory fish. *PNAS* 107:17911-17915.
10. Bergman NM, Lenton TM, & Watson AJ (2004) COPSE: a new model of biogeochemical cycling over Phanerozoic time. *Am. J. Sci.* 304:397-437.
11. Glasspool IJ, Edwards D, & Axe L (2004) Charcoal in the Silurian as evidence for the earliest wildfire. *Geology* 32(5):381-383.
12. Scott AC & Glaspool IJ (2006) The diversification of Paleozoic fire systems and fluctuations in atmospheric oxygen concentration. *Proceedings of the National Academy of Sciences of the United States of America* 103(29):10861-10865.
13. Belcher CM & McElwain JC (2008) Limits for Combustion in Low O_2 Redefine Paleatmospheric Predictions for the Mesozoic. *Science* 321(5893):1197-1200.
14. Hadden RM, Rein G, & Belcher CM (2013) Study of the competing chemical reactions in the initiation and spread of smouldering combustion in peat. *Proceedings of the Combustion Institute* 34(2):2547-2553.
15. Berner RA & Raiswell R (1983) Burial of organic carbon and pyrite sulfur in sediments over phanerozoic time: a new theory. *Geochimica et Cosmochimica Acta* 47(5):855-862.
16. Kump LR (2014) Hypothesized link between Neoproterozoic greening of the land surface and the establishment of an oxygen-rich atmosphere. *Proceedings of the National Academy of Sciences* 111(39):14062-14065.
17. Saltzman MR & Thomas E (2012) Chapter 11 - Carbon Isotope Stratigraphy. *The Geologic*

Experimental P weathering calculation: In our previously reported (20) weathering experiments with granite, the mean amounts of phosphate weathered into aqueous solution were: control microcosms = 0.0137 $\mu\text{mol P}$, biotic microcosms = 0.0726 $\mu\text{mol P}$. The mean moss biomass in the biotic microcosms was 14.390 mg, which assuming 0.43 gC/g biomass and $C/P = 2000$ (table S3) suggests 0.26 $\mu\text{mol P}$ in biomass, or for $C/P = 1000-4000$, 0.13-0.52 $\mu\text{mol P}$ in biomass. This gives a biotic P weathering amplification factor ~ 24 (range 15-43), whereas previously we suggested up to 60 (20). Clearly these estimates are dominated by the unmeasured P content of biomass. However, the P weathering amplification factor has to be > 5.3 (the ratio of dissolved phosphate entering solution in microcosms with moss to those without), which is already considerably greater than the amplification factors for $\text{Ca} = 1.4$ and $\text{Mg} = 1.5$ from granite, indicating selective weathering of P.

COPSE model: We used the COPSE model (10, 20) to study the effects of the early rise of land plants on the coupled biogeochemical cycles of C, O, N, P and S, including the $\delta^{13}\text{C}$ record. The model is described in full in (10) and the version used here incorporates the changes in model structure described in (20). The model has several forcing parameters, including solar luminosity, the geological factors degassing (D), and uplift (U), and the biological forcing factors evolution/colonization (E), enhancement of weathering (W), selective phosphorus weathering (F), and changes to the C/P burial ratio of terrestrially-derived material (CP). The geologic and biologic forcing factors are all normalized to 1 at the present day, except $C/P = 1000$ at present day. Our overall modelling strategy was to try and reproduce key changes in the $\delta^{13}\text{C}$ record with plausible biological and geological forcing scenarios, constrained where possible by available data. We focused initially on altering the biological forcing scenario whilst using the original geological forcing scenario. Then in a sensitivity analysis we considered uncertainty in geologic forcing (91), and alternative initial conditions (altering the feedback structure of the model). The forcing scenarios and sensitivity analyses are detailed in the SI Materials and Methods.

Acknowledgements:

We thank two anonymous referees for their insightful comments that improved the manuscript. T.M.L., S.J.D. and B.M. were supported by the Leverhulme Trust (RPG-2013-106). T.M.L. was also supported by NERC (NE/I005978/2) and by a Royal Society Wolfson Research Merit Award. B. M. was also supported by a University of Leeds Academic Fellowship. T.W.D. was supported by the VILLUM Foundation (VKR023127). Author contributions: T.M.L. designed research. T.M.L. and P.P. performed modelling. S.J.D., B.M. and K.O. helped develop the COPSE model and scenarios. T.W.D., M.R.S., K.O. and P.P. provided data and helped analyze it. T.M.L. wrote the paper with input from all co-authors.

18. Kenrick P, Wellman CH, Schneider H, & Edgecombe GD (2012) A timeline for terrestrialization: consequences for the carbon cycle in the Palaeozoic. *Phil. Trans. B* 367(1588):519-536.
19. Edwards D, Morris JL, Richardson JB, & Kenrick P (2014) Cryptospores and cryptophytes reveal hidden diversity in early land floras. *New Phytologist* 202(1):50-78.
20. Lenton TM, Crouch M, Johnson M, Pires N, & Dolan L (2012) First plants cooled the Ordovician. *Nature Geoscience* 5(2):86-89.
21. Quirk J, et al. (2015) Constraining the role of early land plants in Palaeozoic weathering and global cooling. *Proceedings of the Royal Society of London B: Biological Sciences* 282(1813).
22. Lenton TM & Watson AJ (2000b) Redfield revisited: 2. What regulates the oxygen content of the atmosphere? *Global Biogeochemical Cycles* 14(1):249-268.
23. Robinson JM (1990) Lignin, land plants, and fungi: Biological evolution affecting Phanerozoic oxygen balance. *Geology* 15:607-610.
24. Nelsen MP, DiMichele WA, Peters SE, & Boyce CK (2016) Delayed fungal evolution did not cause the Paleozoic peak in coal production. *Proceedings of the National Academy of Sciences* 113(9):2442-2447.
25. Gerrienne P, et al. (2011) A Simple Type of Wood in Two Early Devonian Plants. *Science* 333(6044):837.
26. Labeeuw L, Martone P, Boucher Y, & Case R (2015) Ancient origin of the biosynthesis of lignin precursors. *Biol Direct* 10(1):1-21.
27. Montañez IP (2016) A Late Paleozoic climate window of opportunity. *Proceedings of the National Academy of Sciences* 113(9):2334-2336.
28. Kennedy KL, et al. (2013) Lower Devonian coaly shales of northern New Brunswick, Canada: plant accumulations in the early stages of Terrestrial colonization. *Journal of Sedimentary Research* 83(12):1202-1215.
29. Porada P, Weber B, Elbert W, Poschl U, & Kleidon A (2013) Estimating global carbon uptake by lichens and bryophytes with a process-based model. *Biogeochemistry* 10(11):6989-7033.
30. Porada P, Weber B, Elbert W, Pöschl U, & Kleidon A (2014) Estimating impacts of lichens and bryophytes on global biogeochemical cycles. *Global Biogeochemical Cycles*:DOI: 10.1002/2013GB0004705.
31. Pohl A, Donnadiou Y, Le Hir G, Buoncristiani JF, & Vennin E (2014) Effect of the Ordovician paleogeography on the (in)stability of the climate. *Clim. Past* 10(6):2053-2066.
32. Porada P, et al. (2016) High potential for weathering and climate effects of non-vascular vegetation in the Late Ordovician. *Nature Communications* 7:10.1038/ncomms12113.
33. Edwards D, Cherns L, & Raven JA (2015) Could land-based early photosynthesizing ecosystems have bioengineered the planet in mid-Palaeozoic times? *Palaeontology* 58(5):803-837.
34. Wang M, Moore TR, Talbot J, & Richard PJH (2014) The cascade of C:N:P stoichiometry in

681	an ombrotrophic peatland: from plants to peat. <i>Environmental Research Letters</i> 9(2):024003.	
682	35. Pope MC & Steffen JB (2003) Widespread, prolonged late Middle to Late Ordovician upwelling in North America: A proxy record of glaciation? <i>Geology</i> 31(1):63-66.	749
683	36. Maikowski K & Racki G (2009) A global biogeochemical perturbation across the Silurian-Devonian boundary: Ocean-continent-biosphere feedbacks. <i>Palaogeography, Palaeoclimatology, Palaeoecology</i> 276(1-4):244-254.	750
684	37. Van Cappellen P & Ingall ED (1996) Redox stabilisation of the Atmosphere and Oceans by Phosphorus-Limited Marine Productivity. <i>Science</i> 271:493-496.	751
685	38. Prokoph A, Shields GA, & Veizer J (2008) Compilation and time-series analysis of a marine carbonate $\delta^{18}O$, $\delta^{13}C$, $87Sr/86Sr$ and $\delta^{34}S$ database through Earth history. <i>Earth-Science Reviews</i> 87(3-4):113-133.	752
686	39. Gill BC, Lyons TW, & Saltzman MR (2007) Parallel, high-resolution carbon and sulfur isotope records of the evolving Paleozoic marine sulfur reservoir. <i>Palaogeography, Palaeoclimatology, Palaeoecology</i> 256(3-4):156-173.	753
687	40. Jones DS & Fike DA (2013) Dynamic sulfur and carbon cycling through the end-Ordovician extinction revealed by paired sulfate-pyrite $\delta^{34}S$. <i>Earth and Planetary Science Letters</i> 363:144-155.	754
688	41. Algeo TJ, Luo GM, Song HY, Lyons TW, & Canfield DE (2015) Reconstruction of secular variation in seawater sulfate concentrations. <i>Biogeosciences</i> 12(7):2131-2151.	755
689	42. Poulsen CJ, Tabor C, & White JD (2015) Long-term climate forcing by atmospheric oxygen concentrations. <i>Science</i> 348(6240):1238-1241.	756
690	43. Kump LR (1988) Terrestrial feedback in atmospheric oxygen regulation by fire and phosphorus. <i>Nature</i> 335:152-154.	757
691	44. Rimmer SM, Hawkins SJ, Scott AC, & Cressler WL (2015) The rise of fire: Fossil charcoal in late Devonian marine shales as an indicator of expanding terrestrial ecosystems, fire, and atmospheric change. <i>American Journal of Science</i> 315(8):713-733.	758
692	45. Glasspool IJ & Scott AC (2010) Phanerozoic concentrations of atmospheric oxygen reconstructed from sedimentary charcoal. <i>Nature Geosci</i> 3(9):627-630.	759
693	46. Diessel CFK (2010) The stratigraphic distribution of inertinite. <i>International Journal of Coal Geology</i> 81(4):251-268.	760
694	47. Glasspool IJ, Scott AC, Waltham D, Pronina NV, & Shao L (2015) The impact of fire on the Late Paleozoic Earth System. <i>Frontiers in Plant Science</i> 6.	761
695	48. Edwards D & Axe L (2004) Anatomical Evidence in the Detection of the Earliest Wildfires. <i>Palaios</i> 19(2):113-128.	762
696	49. Glasspool IJ, Edwards D, & Axe L (2006) Charcoal in the Early Devonian: A wildfire-derived Konservat-Lagerstätte. <i>Review of Palaeobotany and Palynology</i> 142(3-4):131-136.	763
697	50. Pflug HD & Prossl KF (1989) Palynology in Gneiss - Results from the Continental Deep Drilling Program. <i>Naturwissenschaften</i> 76:565-567.	764
698	51. Pflug HD & Prossl KF (1991) Palynostratigraphical and paleobotanical studies in the pilot hole of the German continental deep drilling programme results and implications. <i>Scientific Drilling</i> 2:13-33.	765
699	52. Wollenweber J, et al. (2006) Characterisation of non-extractable macromolecular organic matter in Palaeozoic coals. <i>Palaogeography, Palaeoclimatology, Palaeoecology</i> 240(1-2):275-304.	766
700	53. Peppers RA & Damberger HH (1969) Palynology and Petrography of a Middle Devonian Coal in Illinois. (Illinois State Geological Survey, Urbana, Illinois 61801).	767
701	54. Ammosov IL (1964) Composition pétrographique des charbons humiques de U.R.S.S. <i>CR 5eme Congr. Internat. Stratig. Géol. Carbonif. Paris 9-12 Sept. 1963</i> , Vol 4, pp 1-151.	768
702	55. Volkova IB (1994) Nature and composition of the Devonian coals of Russia. <i>Energy Fuels</i> 8:1489-1493.	769
703	56. Patrakov YF, Kamyarov VF, & Fedyayeva ON (2005) A structural model of the organic matter of Barzas liptobiolith coal. <i>Fuel</i> 84(2-3):189-199.	770
704	57. Sharypov VI, Kuznetsov BN, Beregovtsova NG, Startsev AN, & Parmon VN (2006) Catalytic hydroliquefaction of Barzas liptobiolithic coal in a petroleum residue as a solvent. <i>Fuel</i> 85(7-8):918-922.	771
705	58. Ghorri KAR (1999) Silurian-Devonian petroleum source-rock potential and thermal history, Carnarvon Basin, Western Australia. (Geological Survey of Western Australia, Perth), p 87.	772
706	59. Xu H-H, et al. (2012) Mid Devonian megaspores from Yunnan and North Xinjiang, China: Their palaeogeographical and palaeoenvironmental significances. <i>Palaeworld</i> 21(1):11-19.	773
707	60. Yang Y, Zou R, Shi Z, & Jiang R (1996) <i>Atlas for Coal Petrography of China</i> (China University of Mining and Technology Press, Beijing).	774
708	61. Dai S, Han D, & Chou C-L (2006) Petrography and geochemistry of the Middle Devonian coal from Luquan, Yunnan Province, China. <i>Fuel</i> 85(4):456-464.	775
709	62. Goodarzi F, Gentzis T, & Embry AF (1989) Organic petrology of two coal-bearing sequences from the Middle to Upper Devonian of Melville Island, Arctic Canada. <i>Geological Survey of Canada Paper</i> 89-8:120-130.	776
710	63. Goodarzi F & Goodbody Q (1990) Nature and depositional environment of Devonian coals from western Melville island, Arctic Canada. <i>International Journal of Coal Geology</i> 14(3):175-196.	777
711	64. Gentzis T & Goodarzi F (1991) Petrology, depositional environment and utilization potential of Devonian channel coals from Melville Island, Canadian Arctic Islands. <i>Bulletin de la Societe Geologique de France</i> 162(2):239-253.	778
712	65. Fowler MG, Goodarzi F, Gentzis T, & Brooks PW (1991) Hydrocarbon potential of Middle and Upper Devonian coals from Melville Island, Arctic Canada. <i>Organic Geochemistry</i> 17(6):681-694.	779
713	66. Michelsen JK & Khorasani GK (1991) A regional study on coals from Svalbard; organic facies, maturity and thermal history. <i>Bulletin de la Societe Geologique de France</i> 162(2):385-397.	780
714	67. Rimmer SM, Thompson JA, Goodnight SA, & Robl TL (2004) Multiple controls on the preservation of organic matter in Devonian-Mississippian marine black shales: geochemical and petrographic evidence. <i>Palaogeography, Palaeoclimatology, Palaeoecology</i> 215(1-2):125-154.	781
715	68. Marynowski L & Filipiak P (2007) Water column euxinia and wildfire evidence during deposition of the Upper Famennian Hangenberg event horizon from the Holy Cross Mountains (central Poland). <i>Geological Magazine</i> 144(03):569-595.	782
716	69. Cressler WL (2001) Evidence of earliest known wildfires. <i>Palaios</i> 16(2):171-174.	783
717	70. Rowe NP & Jones TP (2000) Devonian charcoal. <i>Palaogeography Palaeoclimatology Palaeoecology</i> 164(1-4):331-338.	784
718	71. Fairon-Demaret M & Hartkopf-Fröder C (2004) Late Famennian plant mesofossils from the Refrath 1 Borehole (Bergisch Gladbach-Paffrath Syncline; Ardennes-Rhenish Massif, Germany). <i>CFS Courier Forschungsinstitut Senckenberg</i> 251:89-121.	785
719	72. Prestianni C, Decombeix A-L, Thorez J, Fokan D, & Gerrienne P (2010) Famennian charcoal of Belgium. <i>Palaogeography, Palaeoclimatology, Palaeoecology</i> 291(1-2):60-71.	786
720	73. Zhou L, et al. (2011) A new paleoenvironmental index for anoxic events—Mo isotopes in black shales from Upper Yangtze marine sediments. <i>Sci. China Earth Sci.</i> 54(7):1024-1033.	787
721	74. Herrmann AD, et al. (2012) Anomalous molybdenum isotope trends in Upper Pennsylvanian euxinic facies: Significance for use of $\delta^{98}Mo$ as a global marine redox proxy. <i>Chemical Geology</i> 324-325:87-98.	788
722	75. Goldberg T, et al. (2013) Resolution of inter-laboratory discrepancies in Mo isotope data: an intercalibration. <i>Journal of Analytical Atomic Spectrometry</i> 28(5):724-735.	789
723	76. Nägler TF, et al. (2014) Proposal for an International Molybdenum Isotope Measurement Standard and Data Representation. <i>Geostandards and Geoanalytical Research</i> 38(2):149-151.	790
724	77. Canfield DE, Poulton SW, & Narbonne GM (2007) Late-Neoproterozoic Deep-Ocean Oxygenation and the Rise of Animal Life. <i>Science</i> 315:92-95.	791
725	78. Scott C & Lyons TW (2012) Contrasting molybdenum cycling and isotopic properties in euxinic versus non-euxinic sediments and sedimentary rocks: Refining the paleoproxies. <i>Chemical Geology</i> 324-325:19-27.	792
726	79. Dahl TW, et al. (2013) Tracing euxinia by molybdenum concentrations in sediments using handheld X-ray fluorescence spectroscopy (HHXRF). <i>Chemical Geology</i> 360-361:241-251.	793
727	80. Chapin FS, Johnson DA, & McKendrick JD (1980) Seasonal Movement of Nutrients in Plants of Differing Growth Form in an Alaskan Tundra Ecosystem: Implications for Herbivory. <i>Journal of Ecology</i> 68(1):189-209.	794
728	81. Chapin FS (1989) The Cost of Tundra Plant Structures: Evaluation of Concepts and Currencies. <i>The American Naturalist</i> 133(1):1-19.	795
729	82. Chapin FS & Shaver GR (1989) Differences in Growth and Nutrient use Among Arctic Plant Growth Forms. <i>Functional Ecology</i> 3(1):73-80.	796
730	83. Shaver GR & Chapin FS (1991) Production: Biomass Relationships and Element Cycling in Contrasting Arctic Vegetation Types. <i>Ecological Monographs</i> 61(1):1-31.	797
731	84. Aerts R, Verhoeven JTA, & Whigham DF (1999) Plant-Mediated Controls on Nutrient Cycling in Temperate Fens and Bogs. <i>Ecology</i> 80(7):2170-2181.	798
732	85. Riis T, Olesen B, Katborg CK, & Christoffersen KS (2010) Growth Rate of an Aquatic Bryophyte (<i>Warnstorfia fluitans</i> (Hedw.) Loeske) from a High Arctic Lake: Effect of Nutrient Concentration. <i>Arctic</i> 63(1):100-106.	799
733	86. Waite M & Sack L (2011) Does global stoichiometric theory apply to bryophytes? Tests across an elevation x soil age ecosystem matrix on Mauna Loa, Hawaii. <i>Journal of Ecology</i> 99(1):122-134.	800
734	87. Wang M & Moore T (2014) Carbon, Nitrogen, Phosphorus, and Potassium Stoichiometry in an Ombrotrophic Peatland Reflects Plant Functional Type. <i>Ecosystems</i> 17(4):673-684.	801
735	88. Larmola T, et al. (2014) Methanotrophy induces nitrogen fixation during peatland development. <i>Proceedings of the National Academy of Sciences</i> 111(2):734-739.	802
736	89. Delgado V, Ederra A, & Santamaría JM (2013) Nitrogen and carbon contents and $\delta^{15}N$ and $\delta^{13}C$ signatures in six bryophyte species: assessment of long-term deposition changes (1980-2010) in Spanish beech forests. <i>Global Change Biology</i> 19(7):2221-2228.	803
737	90. Elbert W, et al. (2012) Contribution of cryptogamic covers to the global cycles of carbon and nitrogen. <i>Nature Geosci</i> 5(7):459-462.	804
738	91. Royer DL, Donnadieu Y, Park J, Kowalczyk J, & Goddérís Y (2014) Error analysis of CO ₂ and O ₂ estimates from the long-term geochemical model GEOCARBSULF. <i>American Journal of Science</i> 314(9):1259-1283.	805
739		806
740		807
741		808
742		809
743		810
744		811
745		812
746		813
747		814
748		815
		816